Local interval fields for spatial inhomogeneous uncertainty modelling in structural dynamics

R. Callens, M. Faes, D. Moens
KU Leuven, Department of Mechanical Engineering, Division LMSD
Jan De Nayerlaan 5, 2860 St.-Katelijne-Waver, Belgium

Abstract

Interval fields have been introduced to model spatial uncertainty in Finite Element Models when the available data is insufficient to build representative probabilistic models. However, they are limited to modelling global non-stationary uncertainty and hence cannot model local non-stationary uncertainty. This is typically occurring in specific regions of a component or a structure which is produced with,e.g., casting, welding, drawing. This paper presents a more efficient local interval field approach to model the local uncertainty under scarce data. The method is based on the concept of explicit interval fields and aims to develop an alternative approach for the commonly applied inverse distance weighting approach for the generation of the basis functions. In this paper the method is applied on a two-dimensional spatial uncertainty case with a specific focus on dynamics. The paper compares the introduced local interval field approach with inverse distance weighting from a numerical and application point of view.

1 Introduction

Interval analysis is becoming popular when there are only limited or incomplete data of the true model parameters. In comparison to probabilistic techniques, which require distributions of the uncertain parameters, intervals quantify the uncertainty on actual parameter value by an upper and a lower bound. Interval computation methods quantify then, the best and worst-case behavior of the structure. By definition, intervals are independent, and hence, the joint description of several interval-valued parameters is given by a hyper-rectangle [1]. To describe spatial uncertainty with interval Finite Element (FE) analysis, independent intervals are defined on locations in the FE-model (e.g. element centers, element nodes, Gauss points) [2]. The independent intervals neglect all correlation present in the physical quantities under consideration. This results in over-conservative results and unrealistic interval fields due to spurious gradients in the field realisations. To obtain less conservative results, Moens et al. [3] proposed a method to represent spatial uncertainty in FE analyses: interval fields. In this approach, spatial dependency is achieved by limiting the number of intervals to a smaller set of locations (=control points), and defining the relation between those control points and all other locations in the FE-model (e.g., element centers, element nodes, Gauss points) with basis functions [3]. The big advantage of this method is that the dimension of the hyper-rectangle is reduced from the number of all locations in the FE-model to a limited number of interval scalars. These interval fields were recently used for several cases such as modeling of dynamic phenomena [4, 5, 6] and the effect of manufacturing-related uncertainty on the mechanical quality of additive manufactured plastic parts [7]. Another approach to model interval fields is to apply an affine arithmetic representation of the interval uncertainty in combination with the Karhunen-Loève expansion, as presented by Sofi et al. [8] and Sofi and Muscolino [9]. Also, other authors formulated an interval field for static plane stress [10] and an interval field for spatial-time varying uncertainty [11, 12]. Following the explicit interval fields [3], Faes et al. [13] introduced the use of Inverse Distance Weighting (IDW) functions, where the interval scalars are defined on predefined locations in the model domain. In this approach, the local bounds of the interval field at an arbitrary location within the model geometry are computed as a sum of the intervals defined at these control points, weighted with the inverse of their relative distance to this arbitrary location.

However, when considering local inhomogeneous uncertainty, all those interval field techniques are very limited in their ability to model realistic local uncertainty. Local inhomogeneous uncertainty is presented in parts which are for instance deep-drawn or casted. When deep-drawing, there is e.g. local uncertainty in the thickness of the part introduced by local micro cracks and voids. For the cased part, local uncertainty is present inside thicker sections of the part as micro cracks and voids are more likely to be present in those areas due to cooling effects.

In this paper, the description of explicit interval fields [3] is used to model local inhomogeneous spatial uncertainty. As in [13], the interval scalars are defined on locations in the model domain (control points) and the spatial dependency is described with basis functions. The modeling of local inhomogeneous uncertainty is achieved by defining the basis function such that the dependency is limited to a zone around their control point. To construct these basis functions, the technique of IDW from Shepard is modified and combined with a weighting function that satisfies two requirements for local weighting functions.

The paper is structured as follows: section 2 presents interval field FE analysis. This technique is then extended to model intervals fields with basis functions and a limited set of interval scalars using explicit interval fields. Next, in section 3 the method of IDW is described. Section 4 proposes a new local interval field method to model local uncertainty. A structural dynamic academic case study is used to illustrate the difference between the basis functions of IDW [14] and the local interval fields in section 5. At the end of this paper, the conclusions are summarized in section 6.

2   Interval Field Finite Element analysis

In current engineering practice, FE analysis is a popular technique used to approximate the solution of a partial differential equation (PDE). In this work, we consider that FE models are parametric, i.e., they are represented by a numerical model $\mathcal{M}(\boldsymbol{x})$, parameterized by a vector $\boldsymbol{x}(\boldsymbol{r}) \in \mathcal{X} \subsetneq \mathbb{R}^{d_i}$ with $\mathcal{X}$ the admissible set of input parameters and $d_i \in \mathbb{N}$ the number of input parameters. For instance, $\boldsymbol{x}(\boldsymbol{r})$ contains material parameters as a function of the spatial coordinate $\boldsymbol{r} \in \Omega \subsetneq \mathbb{R}^{d_\Omega}$ with $d_\Omega \in \mathbb{N}, d_\Omega \leq 4$ the number of dimensions (max. 3 Cartesian dimensions and 1 time dimension).

The model domain Ω is discretised in N_e elements $\Omega_e \subseteq \Omega$ yielding d_d degrees of freedom (DOF) and the PDE is approximated by the solution of a set of algebraic equations.

The model $\mathcal{M}(\boldsymbol{r})$ provides a vector of model responses $\boldsymbol{y}(\boldsymbol{r}) \in \mathcal{Y} \subsetneq \mathbb{R}^{d_o}$ with $\mathcal{Y}$ the admissible set of output parameters and $d_o \in \mathbb{N}$ the number of output parameters. This is defined as:

$$M(\boldsymbol{x}) : y_i(\boldsymbol{r}) = m_i(\boldsymbol{x}(\boldsymbol{r})) \tag{1}$$

with $m_i : \mathbb{R}^{d_i} \mapsto \mathbb{R}$ mapping the parametric input space to the individual outputs of the FE analysis and $i = 1, 2, \ldots, d_o$, when the output $\boldsymbol{y}$ is generated on element or nodal level $\boldsymbol{r}$ (e.g. displacement, strains). Note that when the output is defined on a global model level (e.g., eigenfrequencies), the outputs y_i are not dependent on $\boldsymbol{r}$.

Spatial uncertainty is here introduced in FE analysis with interval fields [15]. An interval scalar $x^I \in \mathbb{IR}$, where $\mathbb{IR}$ is the domain of closed real-valued intervals, is defined as:

$$x^I = [x_{min} \ x_{max}] = [\underline{x} \ \overline{x}] = \{x \in \mathbb{R} | \underline{x} \leq x \leq \overline{x}\}, \tag{2}$$

with x_{min} and x_{max} bounds of the uncertain parameter x. The midpoint of the interval is defined as:

$$x_\mu = \frac{\underline{x} + \overline{x}}{2}. \tag{3}$$

An interval vector $\boldsymbol{x}^I \in \mathbb{IR}^{d_i}$ contains d_i interval scalars which are by definition independent from each

other. In general, the interval FE analysis [15] has an uncertain interval vector $\boldsymbol{x}^I \in \mathbb{IR}^{d_i}$ as input:

$$\boldsymbol{x}^I = \begin{Bmatrix} x_1^I \\ x_2^I \\ \vdots \\ x_{d_i}^I \end{Bmatrix} = \left\{ \boldsymbol{x} \in \mathbb{R}^{d_i} | x_i \in x_i^I \right\}. \tag{4}$$

The solution set $\boldsymbol{y}^S \in \mathbb{R}^{d_o}$ of the interval FE analysis is then formulated as:

$$\boldsymbol{y}^S = \left\{ \boldsymbol{y} | \left(\boldsymbol{x} \in \boldsymbol{x}^I \right) \left(\boldsymbol{y} = \boldsymbol{m}(\boldsymbol{x}) \right) \right\}, \tag{5}$$

with $\boldsymbol{m}(\boldsymbol{x})$ containing $m_1, \ldots, m_i, m_{d_o}$ the deterministic functions of the FE analysis and $\boldsymbol{y} \in \mathbb{R}^{d_o}$. The solution set $\boldsymbol{y}^S$ is commonly approximated by an interval vector $\boldsymbol{y}^I \in \mathbb{IR}^{d_o}$:

$$\boldsymbol{y}^I = \begin{Bmatrix} y_1^I \\ y_2^I \\ \vdots \\ y_{d_o}^I \end{Bmatrix}. \tag{6}$$

The components $y_i^I = \left[\underline{y}_i\, \overline{y}_i \right]$ of $\boldsymbol{y}^I$ are found by optimisation:

$$\underline{y}_i = \min_{\boldsymbol{x} \in \boldsymbol{x}^I} m_i(\boldsymbol{x}), \tag{7}$$

$$\overline{y}_i = \max_{\boldsymbol{x} \in \boldsymbol{x}^I} m_i(\boldsymbol{x}). \tag{8}$$

With this optimization the interval of each component is found independently, such that the solution set $\boldsymbol{y}^S$ is approximated with a hyper-rectangle.

With explicit interval fields, there are independent intervals scalars $\boldsymbol{\alpha}^I \in \mathbb{IR}^{n_b}$ with $n_b \in \mathbb{N}$, such that the input space is reduced from $\mathbb{IR}^{d_i}$ to $\mathbb{IR}^{n_b}, d_i \geq n_b$. From these interval scalars the dependency inside Ω is modeled with basis functions $\boldsymbol{\psi}_i(\boldsymbol{r}) : \Omega \mapsto \mathbb{R}^{k_{FE}}$ with $i = 1, 2, \ldots, n_b$ and k_{FE} the total number of interval field discretisation points in Ω. An explicit interval field $\boldsymbol{x}^I(\boldsymbol{r}) : \Omega \times \mathbb{IR}^{n_b} \mapsto \mathbb{IR}^{k_{FE}}$ is as such build as a series expansion of n_b basis functions, multiplied with interval scalars:

$$\boldsymbol{x}^I(\boldsymbol{r}) = \sum_{i=1}^{n_b} \boldsymbol{\psi}_i(\boldsymbol{r}) \cdot \alpha_i^I. \tag{9}$$

To propagate the interval field through $\mathcal{M}$ the number of required deterministic model evaluations is important, especially when using industrially-sized FE models (up to millions of DOF). To achieve this, the number of interval scalars d_i must be limited as the number of deterministic model evaluations scale with 2^{d_i} when considering linear monotonic interval analysis. In this perspective, the explicit interval field formulation has the advantage that the input space is reduced from $\mathbb{IR}^{d_i}$ to $\mathbb{IR}^{n_b}, d_i \geq n_b$.

3 Interval fields with Inverse Distance Weighting

Section 2 introduced the description of interval FE analysis and explicit interval fields, where the interval field is built with interval scalars and basis functions. As the basis function determines the spatial dependency of the field, it is of great importance to select a basis function that represents the physical nature of the field. In this work, the approach as presented by Faes et al. [16] is used as a starting point. Basis functions are generated with IDW to describe the spatial dependency from interval scalars that are defined on specific

locations r in the domain Ω. The IDW basis function $\psi_i(r)$ is built from weight functions ${}^{IDW}w_i(r)$:

$$\psi_i(r) = \frac{{}^{IDW}w_i(r)}{\sum\limits_{j=1}^{n_b} {}^{IDW}w_j(r)}, \tag{10}$$

with $r \in \Omega$ and ${}^{IDW}w_i(r)$ the weight functions calculated as:

$$ {}^{IDW}w_i(r) = \frac{1}{[d(r, r_{n_i})]^p}, \tag{11}$$

where $d(r, r_{n_i})$ is the Euclidean distance between the locations $r \in \Omega$ and locations of the control points $r_{n_i} \in \Omega$. The power p controls the gradient and the continuity of the weight function. As a result of the distance calculations, the computational cost of generating the weight functions scales with $O(k_{FE} \times n_b)$, the total number of interval field discretisation points in the FE model k_{FE} and the control points n_b. Here the weight and basis functions are discretised following the element centers, element nodes or Gauss points of the FE-model Ω, resulting in computational cost depending on the number of DOF in the FE-model. However, this computational cost is can be reduced by using sparse grids to reduce the interval field discretisation points, as presented by the authors [17].

From equation 10 and 11, the inverse distance basis functions are strictly positive on all locations of the model that do not coincide with control points, are one at the defining control point location r_{n_i} and are zero at all other control points (global dependency). The global dependency is achieved through the weighting functions and through the following properties:

1. $\dfrac{\partial\, {}^{IDW}w_i}{\partial d(r, r_{n_i})} \leq 0$ and when $d(r, r_{n_i}) \to \infty : \dfrac{\partial w_i}{\partial d(r, r_{n_i})} \to 0$,

2. $\begin{cases} {}^{IDW}w_i(r) \geq 0 & \text{if} \quad d(r, r_{n_i}) \neq \infty, \\ {}^{IDW}w_i(r) = 0 & \text{if} \quad d(r, r_{n_i}) = \infty, \end{cases}$

those properties are only valid when the size of the FE $h_e \to 0$. As a result, this weighting technique with global dependency is not capable to describe local dependency, as through the second property, all weight functions will contribute to non-zero uncertainty levels throughout the entire spatial domain. An idea could be to truncate the basis functions on a distance from the control points. The disadvantage of truncating is that it introduces discontinuities in the field. Another idea is to use other weighting functions that are zero on a finite distance of a control point. In the next section of this paper the use of a local weighting and basis function is presented.

4 Interval field with local dependency

An explicit interval field has local dependency if it is built from weighting functions w_i that satisfy the following properties:

1. $\dfrac{\partial w_i}{\partial d(r, r_{n_i})} \leq 0$ and when $d(r, r_{n_i}) \to R_i : \dfrac{\partial w_i}{\partial d(r, r_{n_i})} \to 0$,

2. $\begin{cases} w_i(r) \neq 0 & \text{if} \quad d(r, r_{n_i}) < R_i, \\ w_i(r) = 0 & \text{if} \quad d(r, r_{n_i}) \geq R_i, \end{cases}$

those properties are only valid when the size of the FE $h_e \to 0$, with R_i the width of the support zone $\Omega_i \subseteq \Omega$ where $i = 1, \dots, d_\Omega$ and $d_\Omega \leq 4$ around one control point n_i. The first property ensures that the weighting

function is monotonically decreasing to zero on the edge of the support zone Ω_i. Property two introduce the local description of the weight function, specifying that the weight function is zero starting from a distance $\boldsymbol{R}_i$ around the control point n_i

The local character of the weight function introduces the following computational advantage in comparison to IDW. The support zone $\Omega_i \in \Omega$ where $\boldsymbol{d}(\boldsymbol{r}, \boldsymbol{r}_{n_i}) < \boldsymbol{R}_i \rightarrow \boldsymbol{w}_i(\boldsymbol{r}) \neq 0$ is compact $\mathbb{K}$ such that it is closed and bounded. This means that the weight function must only be calculated inside Ω_i and not on the full domain Ω, yielding a drastic gain in computational efficiency as k_{FE} is reduced to a very limited set of discretisation points.

Further in this paper, the support zone Ω_i of one control points n_i is defined as $\mathcal{K}$. Weight functions are then $\boldsymbol{w}^{\mathcal{K}}(\boldsymbol{r}) : \mathcal{K} \mapsto \mathbb{R}^{k_{FE}}$ and basis functions are $\boldsymbol{\psi}^{\mathcal{K}}(\boldsymbol{r}) : \mathcal{K} \mapsto \mathbb{R}^{k_{FE}}$. Paragraph 4.1 describes the construction of basis functions for 1D ($d_\Omega = 1$) as recently introduced by the authors in [18].

4.1   Local basis functions for 1-dimensional domains

To build local basis functions $\boldsymbol{\psi}^{\mathcal{K}}(\boldsymbol{r}) : \mathcal{K} \mapsto \mathbb{R}^{k_{FE}}$ from weight functions, equation 10 is changed. In this equation, the weight functions are normalized to the weight functions of other control points. As there is only one control point and weight function inside the domain $\mathcal{K}$, the weight function $\boldsymbol{w}^{\mathcal{K}}(\boldsymbol{r})$ is normalized to itself and the basis function $\boldsymbol{\psi}^{\mathcal{K}}(\boldsymbol{r})$ is a constant function equal to one inside $\mathcal{K}$. This results in a discontinuous basis function: one inside $\mathcal{K}$ and zero outside $\mathcal{K}$. A continuous basis function is achieved by adding two virtual nodes $n^{\mathcal{K}}$ on the edges of each spatial dimension of the domain $\mathcal{K}$. For a one-dimensional problem, the nodes inside $\mathcal{K}$ are located on:

1. the lower bound edge of $\mathcal{K}$: $\boldsymbol{r}^{\mathcal{K}}_{n=1} = \boldsymbol{r}_{n_i} - R$,

2. the midpoint of $\mathcal{K}$: $\boldsymbol{r}^{\mathcal{K}}_{n=2} = \boldsymbol{r}_{n_i}$,

3. the upper bound edge of $\mathcal{K}$: $\boldsymbol{r}^{\mathcal{K}}_{n=3} = \boldsymbol{r}_{n_i} + R$,

with the first and last virtual node on the edges of $\mathcal{K}$ and $\boldsymbol{r}_{n_i} \in \mathcal{K}$ the location of the control point n_i. On all those virtual nodes, weighting functions are defined $\boldsymbol{w}^{\mathcal{K}}_i(\boldsymbol{r})$ with $i = 1, 2, 3$ for 1D. This is visualised in figure 1, which illustrates the building of one basis function inside $\mathcal{K}$ from the weight functions (in this figure, quartic splines are used see section 5.2). The result is a basis function which is continuous in $\mathcal{K}$ and has a local spatial dependency.

Using those virtual nodes and control point in $\mathcal{K}$ equation 10 is changed to:

$$\boldsymbol{\psi}^{\mathcal{K}}(\boldsymbol{r}^{\mathcal{K}}) = \boldsymbol{a}^{\mathcal{K}} \frac{\boldsymbol{w}^{\mathcal{K}}_i(\boldsymbol{r}^{\mathcal{K}})}{\displaystyle\sum_{j=1}^{3} w^{\mathcal{K}}_j(\boldsymbol{r}^{\mathcal{K}})}, \tag{12}$$

with $\boldsymbol{r}^{\mathcal{K}} \in \mathcal{K} \subseteq \Omega$ and $\boldsymbol{a}^{\mathcal{K}}$ is defined as:

$$\boldsymbol{a}^{\mathcal{K}} = \begin{cases} 1 \text{ if } \boldsymbol{r}^{\mathcal{K}}_n = \boldsymbol{r}_{n_i} \\ 0 \text{ if } \boldsymbol{r}^{\mathcal{K}}_n \neq \boldsymbol{r}_{n_i}, \end{cases} \tag{13}$$

with $\boldsymbol{r}^{\mathcal{K}}_n$ the locations of the nodes in $\mathcal{K}$ and $\boldsymbol{r}_{n_i}$ the location of the control point n_i in Ω. The definition of $\boldsymbol{a}^{\mathcal{K}}$ is such that the basis function of the control point n_i is retained from all the basis functions of the nodes inside $\mathcal{K}$.

The basis function $\boldsymbol{\psi}^{\mathcal{K}}(\boldsymbol{r}^{\mathcal{K}})$ is then mapped from the domain $\mathcal{K}$ to the domain Ω by the locations of, e.g., element nodes, element centers or Gauss points using:

$$\boldsymbol{\psi}_i(\boldsymbol{r}) = \begin{cases} \boldsymbol{\psi}^{\mathcal{K}}(\boldsymbol{r}^{\mathcal{K}}) & \text{if } \mathcal{K}_e = \Omega_e \\ 0 & \text{if } \mathcal{K}_e \neq \Omega_e. \end{cases} \tag{14}$$
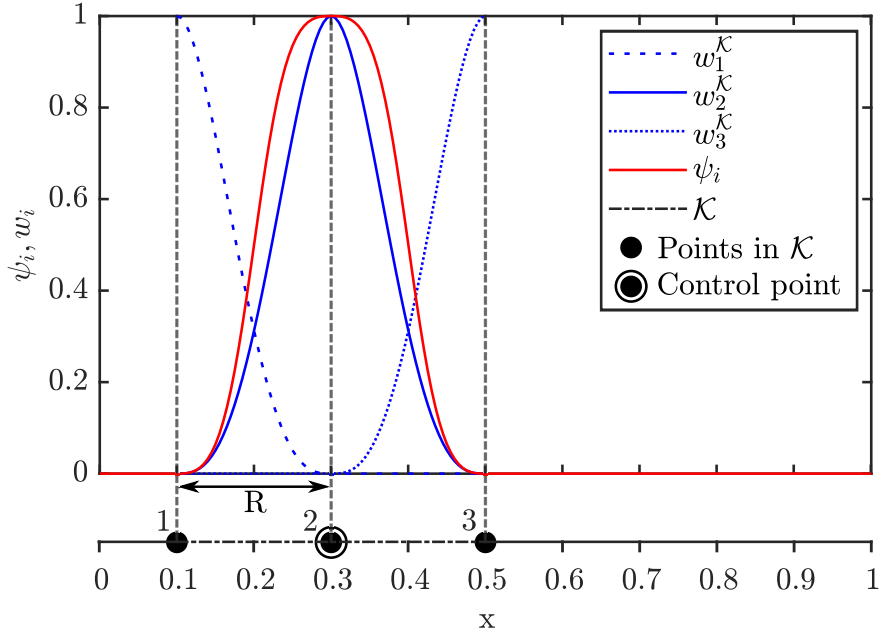
Figure 1: For a 1D domain, the location of the virtual control points (small black dots) and control point (big black dot). The corresponding weight functions (quartic spline) and basis function are visualised in blue and red. R describes the width of the domain $\mathcal{K}$ around the control point.

The basis function $\boldsymbol{\psi}_i(\boldsymbol{r}) \in \Omega$ is zero outside $\mathcal{K}$ such that strict local dependency is obtained. The interval field is then represented as:

$$\boldsymbol{x^I}(\boldsymbol{r}) = \boldsymbol{x}_\mu + \sum_{i=1}^{n_b} \boldsymbol{\psi}_i(\boldsymbol{r}) \cdot (\boldsymbol{\alpha}_i^I - \boldsymbol{x}_\mu), \tag{15}$$

where $\boldsymbol{x}_\mu$ is the midpoint of the field. The previous methodology is valid as long as the weight function satisfies the three properties. As a result, an interval field with local influence is reached.

4.2 Local basis functions for two-dimensional domains

For problems which have $d_\Omega = 2$, the construction of a multidimensional weight function is necessary. This construction is depending on the node structure in $\mathcal{K}$. In this paper the proposed structure is a rectangle. Computationally a rectangular is the most efficient way, as the locations in FE-models are commonly defined in a Cartesian coordinate system. The node structure is visualized for $d_\Omega = 2$ in figure 2. This rectangle domain is only valid if the uncertainty under consideration is concentrated inside a rectangle. Otherwise, different structures have to be defined, where a coordinate transformation is necessary. This, however, is outside the scope of this paper. With this node structure, the weight function in $d_\Omega = 2$ is constructed by a Kronecker product of six weight function defined where three weight functions are defined on each spatial dimension, such that the required two-dimensional distance calculation is reduced to two one-dimensional distance calculations. The location for each node in $\mathcal{K}$ is the same as when $d_\Omega = 1$. This limits the required distance measures to two one-dimensional problems. In practice, distance calculations are required between the coordinates of the control points n_i and the FE nodes, element centers or Gauss points. Using a Cartesian space $d_\Omega = 2$, the normalized distances are calculated with equation 7 in each dimension of $\mathcal{K}$:

$$\bar{\boldsymbol{d}}_{x_i} = \frac{\boldsymbol{d}(\boldsymbol{r}_{x_i}, \boldsymbol{n}_{x_i}^{\mathcal{K}})}{R_{x_i}}, \tag{16}$$

$$\bar{\boldsymbol{d}}_{y_i} = \frac{\boldsymbol{d}(\boldsymbol{r}_{y_i}, \boldsymbol{n}_{y_i}^{\mathcal{K}})}{R_{y_i}}. \tag{17}$$
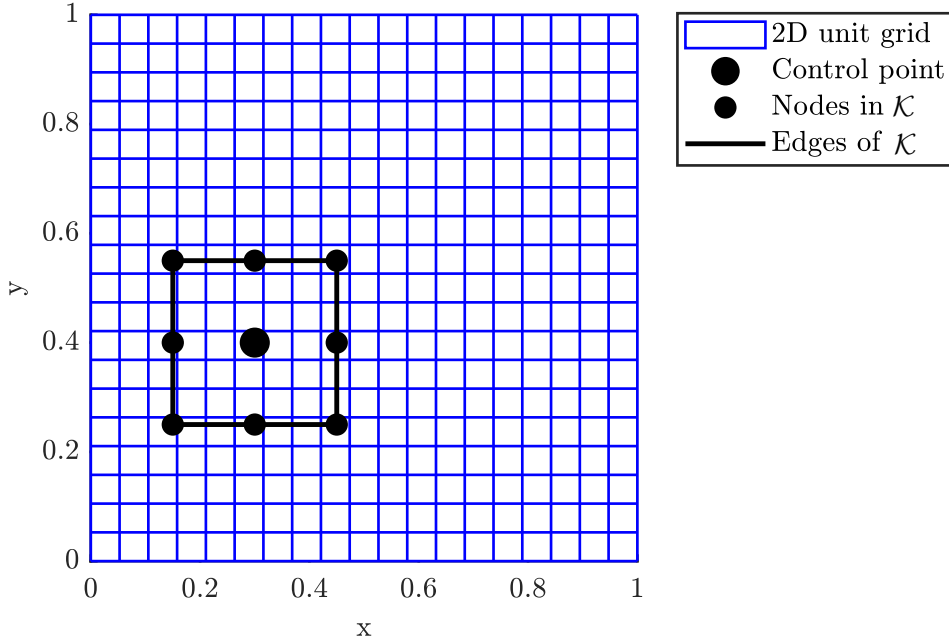
Figure 2: 2D unit grid of 20×20 in blue, where one control point is defined on the midpoint of domain $\mathcal{K}$: coordinate $(0.3; 0.4)$. The edges of the domain $\mathcal{K}$ show the width of the domain in black with dimensions: $R_x, R_y = 0.15$. The smaller black nodes are the virtual nodes defined in $\mathcal{K}$ on which the weight and basis functions are defined.

If the weight function is defined by the analyst, they can be calculated for each dimension of $\mathcal{K}$ with the normalised distances. In two dimensions the resulting weight functions are $\boldsymbol{w}_{x_i}^{\mathcal{K}}, \boldsymbol{w}_{y_i}^{\mathcal{K}}$. By using the Kronecker product of those six weight functions (three in each dimension), on each node in $\mathcal{K}$, a two dimensional weight function is obtained:

$$\boldsymbol{w}_{xy_i}^{\mathcal{K}} = \boldsymbol{w}_{x_i}^{\mathcal{K}} \otimes \boldsymbol{w}_{y_i}^{\mathcal{K}}. \tag{18}$$

The resulting weight functions inside $\mathcal{K}$ are visualized in figure 3. The basis function generated with equations 12 and 13 for one control point and one interval is visualized in figure 4 and the resulting interval field is then calculated by using equations 14 and 15.

5 Case study: Interval Field on a 2D plate

In this case-study, the effect of local material uncertainty on the first bending mode of a rectangular plate clamped at one side is studied. Additionally, the difference between local explicit interval field and explicit interval field with IDW is shown. For the local explicit interval fields, the weighting functions are defined as quartic splines as these satisfy the two necessary properties for the definition of a local explicit interval field.

5.1 Problem description

This case study concerns an interval field that is calculated for a 2D FE linear elastic model of a square plate, which is $L = 1\,\text{m}$ long and wide. The plate is uniformly discretised with square elements of size $h = 0,0125\,\text{mm}$, resulting in 6400 elements. The boundary condition is modeled as a Dirichlet boundary condition with for $y = 0 : u = 0\,\text{mm}$. The plate has a uniform thickness of $t = 25\,\text{mm}$. Figure 5 visualizes the plate with its boundary conditions.
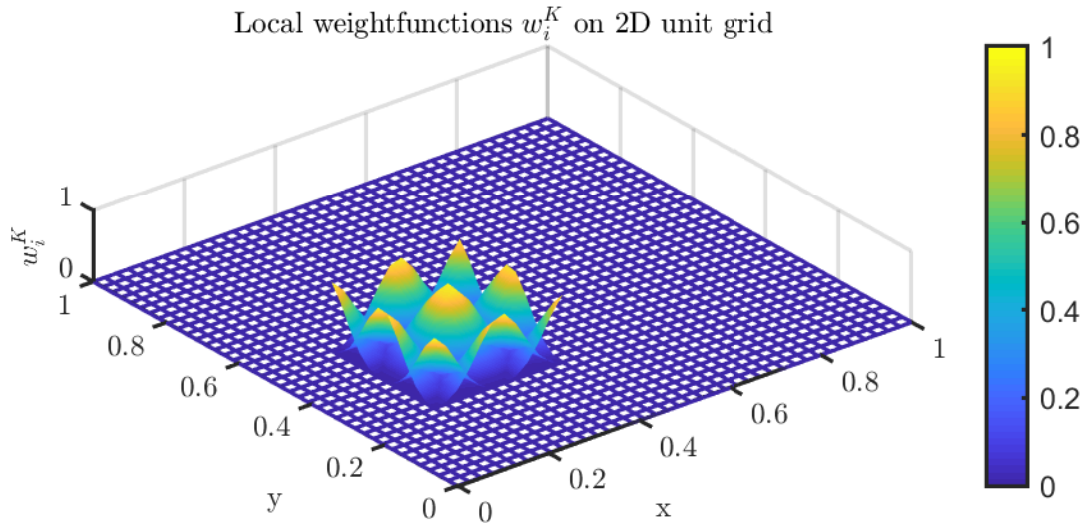
Figure 3: 2D unit grid of 20×20 in blue, where the weighting functions are defined on $\mathcal{K}$
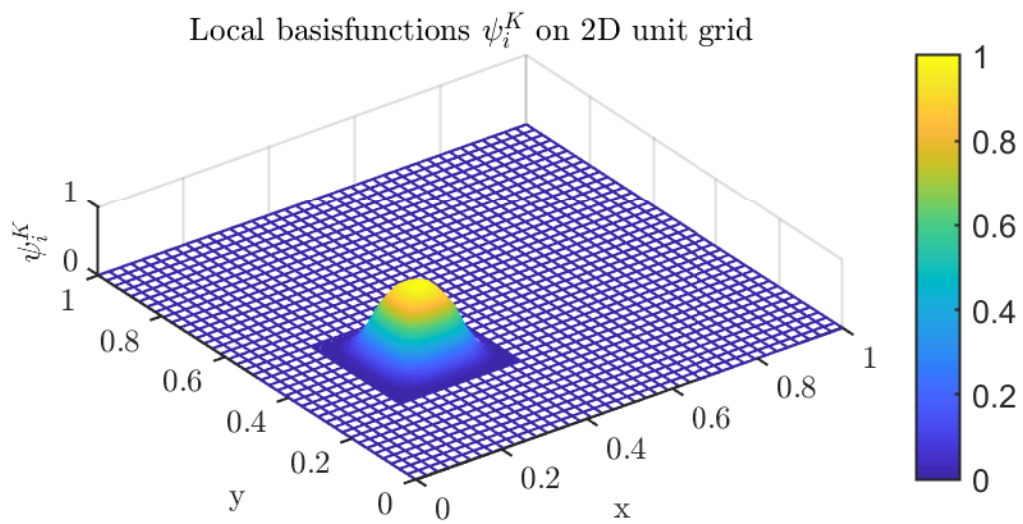
Figure 4: 2D unit grid of 20×20 in blue, where the basis function is defined on $\mathcal{K}$
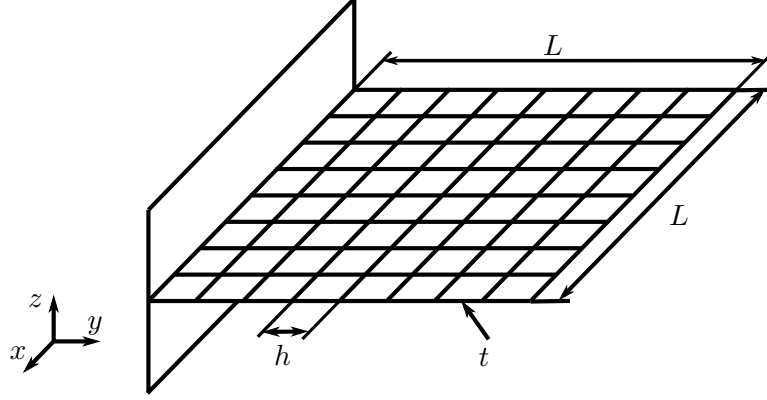
Figure 5: 2D case: the linear elastic square plate of length $L = 1\,\mathrm{m}$ is discretised in 6400 square elements of size $h = 0,0125\,\mathrm{mm}$. Boundary conditions are: fixed displacement for $y = 0 : u = 0\,\mathrm{mm}$. The plate has a uniform thickness of $t = 25\,\mathrm{mm}$

The uncertainty is defined as an interval field on the Young's modulus using two control points. Table 1 gives the coordinates (x_i, y_i) of those control points, the interval values E_i^I and the width R_{xi}, R_{yi} of the domain $\mathcal{K}$ around each control point.

Table 1: Uncertainty in 3 control points with location, intervals E_i^I and width of the local domain $\mathcal{K}$ around each control point i

Control point	Location (x_i, y_i) (m)	Intervals E_i^I (GPa)	Width (R_{xi}, R_{yi}) (m)
1	$(0.2, 0.3)$	$[50, 90]$	$(0.1, 0.15)$
2	$(0.8, 0.1)$	$[50, 90]$	$(0.2, 0.1)$

5.2 Explicit interval field for global or local uncertainty modeling

Explicit interval fields allow to select basis functions that represent the spatial uncertainty of the component or structure, such that the expert is able to choose between global or local dependency. For global dependency the basis functions obtained with IDW give a smooth continuous function that is always greater then zero expect in the control points where its zero. The formulation of an explicit interval field with IDW is given in section 3. From equation 10 the IDW functions $^{IDW}w_i \in \Omega$ are calculated and the basis functions $\psi_i \in \Omega$ are obtained with equation 11. In addition to the values in table 1 the value of the power factor p of IDW is chosen as $p = 2$.

Local dependency is on the other hand achieved by selection of the weighting function, this is limited by the two properties in section 4. The used weight function in this paper is a quartic spline $^Q w_i^{\mathcal{K}}$ from [19] based on the Euclidean distance between the location $r_n^{\mathcal{K}}$ of the nodes $n^{\mathcal{K}}$ and the locations $r^{\mathcal{K}}$. This distance is then normalized with the support width R:

$$\bar{d}(r_n^{\mathcal{K}}, r^{\mathcal{K}}) = \frac{d(r_n^{\mathcal{K}}, r^{\mathcal{K}})}{R}. \tag{19}$$

At a distance R of the nodes $n^{\mathcal{K}}$ the normalized distance equals zero and the functions is monotonically decreasing, as visualised in figure 1. This can be verified when the weight functions are analytically expressed as:

$$^Q w_i^{\mathcal{K}}(\bar{d}) = \begin{cases} 1 - 6\bar{d}(r_n^{\mathcal{K}}, r^{\mathcal{K}})^2 + 8\bar{d}(r_n^{\mathcal{K}}, r^{\mathcal{K}})^3 - 3\bar{d}(r_n^{\mathcal{K}}, r^{\mathcal{K}})^4 & \bar{d}(r_n^{\mathcal{K}}, r^{\mathcal{K}}) \leq 1 \\ 0 & \bar{d}(r_n^{\mathcal{K}}, r^{\mathcal{K}}) > 1. \end{cases} \tag{20}$$

Three local weight functions $w_{x_i}^{\mathcal{K}}, w_{y_i}^{\mathcal{K}}$ (quartic splines) are first calculated for each dimension separately with equation 19, equation 20 and the values from table 1. From those weight functions, two dimensional
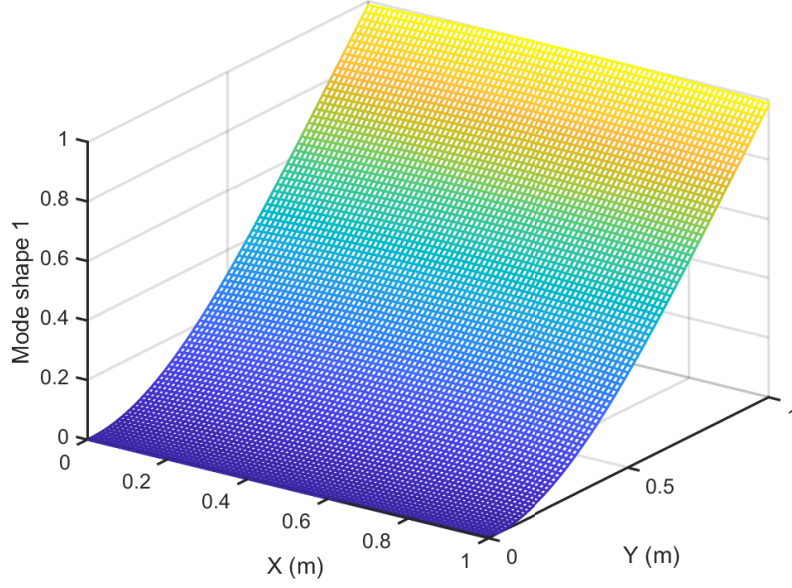
Figure 6: The first bending mode of a 2D plate with deterministic input field with constant Young's Modulus of $E = 70GPa$

weight functions are calculated with equation 18 and the basis functions $\psi^{\mathcal{K}}$ with equation 12. The resulting weight and basis functions inside $\mathcal{K}$ are similar to the one visualised in respectively figure 3 and figure 4. The basis functions are then mapped from the local domain $\mathcal{K}$ to the model domain Ω with equation 14.

5.3 First bending mode with local uncertainty on the Young's modulus

The changes in the first bending mode are characterized when comparing the first bending mode with $M_1^U(x, y)$ and without $M_1^D(x, y)$ spatial uncertainty for the 2D plate with a local interval field as defined in 5.2. The difference $D_1(x, y)$ in percent is then calculated with the following equation:

$$D_1(x, y) = 100\% \cdot \frac{M_1^D(x, y) - M_1^U(x, y)}{\max\limits_{x,y \in \Omega} \left(M_1^D(x, y) \right)}, \tag{21}$$

where, the difference between de deterministic $M_1^D(x, y)$ and uncertainty $M_1^U(x, y)$ bending mode is scaled with the maximum value $\max\limits_{x,y \in \Omega} \left(M_1^D(x, y) \right)$ of the deterministic bending mode. Figure 6 visualises the deterministic first bending mode shape $M_1^D(x, y)$ scaled by its maximum value, for the deterministic input field with a constant Young's Modulus of $E = 70GPa$.

Propagating the spatial uncertainty is limited to the vertex analysis, as for this specific case the interval field analysis is strictly monotonic. Consequently, the highest difference $D_1(x, y)$ on the first bending mode is obtained when the interval parameters are at a corner of the vertex interval domain. The difference $D_1(x, y)$ is visualized in figure 7 on the right side, along with the corresponding vertex realisations on the left side. The overall difference is small $D_1(x, y) < 1\%$ with the highest value at location $y = 1$. In the regions where local uncertainty is defined, a relatively small $D_1(x, y) < 0.2\%$ difference is noticeable, when y increases away from those regions the difference raises until the maximum when $y = L$. In all those realizations, the uncertainty introduces a small torsional change into the first bending mode, which is smaller for the first and last realisation. For the second and third realisation, the change in Young's modulus inside the plate is at maximum value and so the torsional effect for this particular case is also at its maximum value.
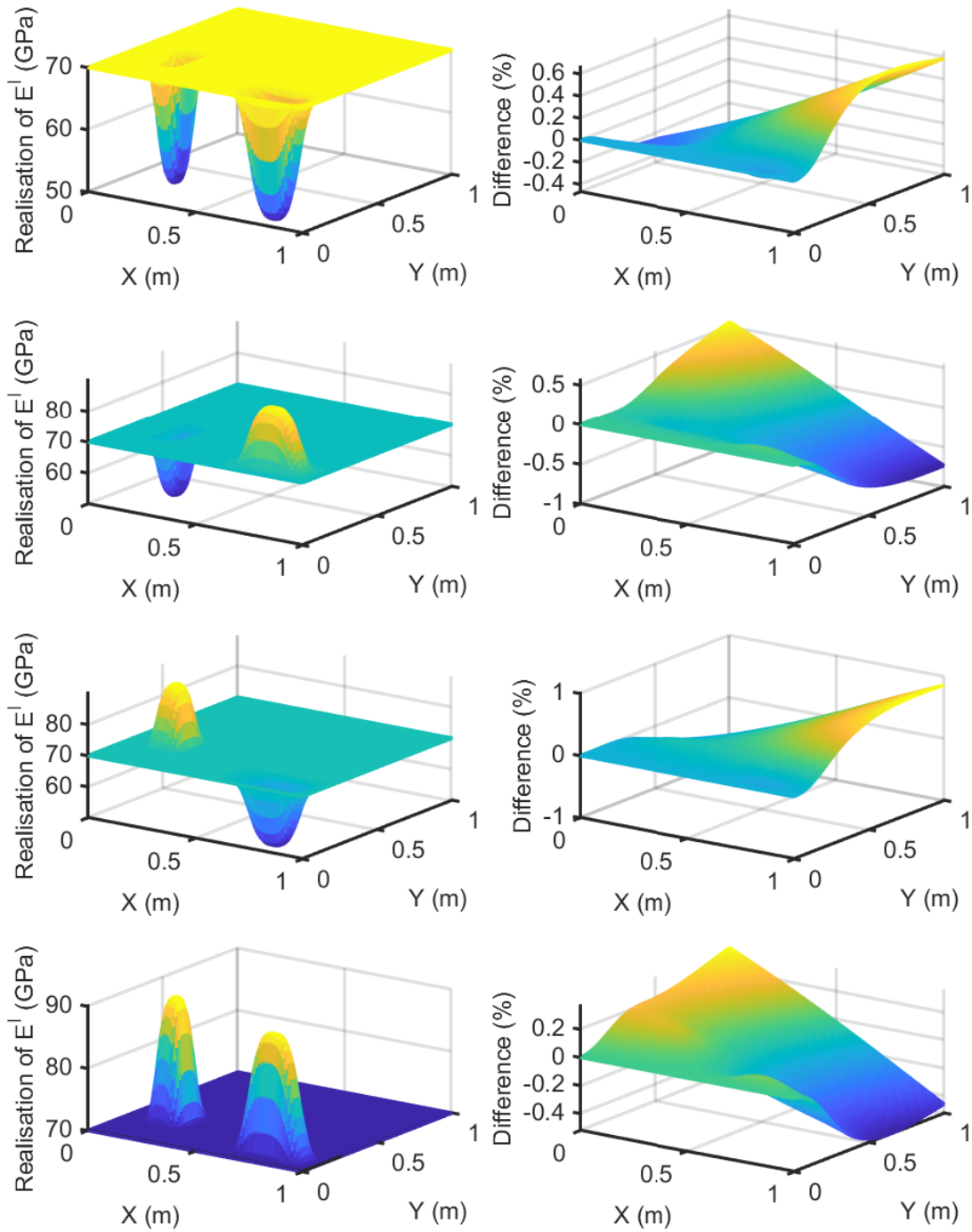
Figure 7: Left the interval field realisations of the input field $\boldsymbol{E}^I$. Right the difference $D_1(x, y)$ between the deterministic first bending mode and the first bending mode corresponding to the interval field realisations

5.4 Interval field propagation

The explicit interval field realizations are calculated form the basis functions (see subsection 5.2) and equation 15 with $\alpha_i^I = E_i^I$ and $\boldsymbol{x}_\mu = \boldsymbol{E}_\mu$ the midpoint of the field. To quantify the interval of the first three eigenfrequencies f_1^I, f_2^I, f_3^I the interval field $\boldsymbol{E}^I$ is propagated.

The 2D plate is linear-elastic and so the interval analysis problem is monotonic and especially strictly positive monotonic for this specific case, as the basis functions are stationary and a higher Young's modulus will result in a higher eigenfrequency. As a result, the intervals of the eigenfrequencies f_1^I, f_2^I, f_3^I are quantified by solving the FE-model with two realisations of the interval field. Each realisation has different interval field scalars:

- interval field scalars for the highest eigenfrequencies $\overline{y}$:
    1. $E_1^I : \overline{E}_1 = 90\,\text{Gpa}$,
    2. $E_2^I : \overline{E}_2 = 90\,\text{Gpa}$.

- interval field scalars for the lowest eigenfrequencies $\underline{y}$:
    1. $E_1^I : \underline{E}_1 = 50\,\text{Gpa}$,
    2. $E_2^I : \underline{E}_2 = 50\,\text{Gpa}$.

The resulting intervals on the first three eigenfrequencies for local explicit interval fields with quartic splines is:

$$^Q f_1^I = \left[\underline{f}_1, \overline{f}_1\right] = [20.88, 21.35]\,(Hz), \tag{22}$$

$$^Q f_2^I = \left[\underline{f}_2, \overline{f}_2\right] = [50.73, 51.37]\,(Hz), \tag{23}$$

$$^Q f_3^I = \left[\underline{f}_3, \overline{f}_3\right] = [129.75, 130.87]\,(Hz), \tag{24}$$

and for IDW the interval is:

$$^{IDW} f_1^I = \left[\underline{f}_1, \overline{f}_1\right] = [17.86, 23.97]\,(Hz), \tag{25}$$

$$^{IDW} f_2^I = \left[\underline{f}_2, \overline{f}_2\right] = [43.16, 57.90]\,(Hz), \tag{26}$$

$$^{IDW} f_3^I = \left[\underline{f}_3, \overline{f}_3\right] = [110.17, 147.82]\,(Hz). \tag{27}$$

The difference in basis functions used in the local interval field and the global IDW interval field introduces the change in intervals of the eigenfrequenties. When only local uncertainty is present in the component, the local uncertainty modeling technique will be clearly less conservative then the global uncertainty modeling technique.

5.5 Difference in computational cost

The computational cost in interval analysis is most often concentrated in propagating the uncertainty and less in modelling the field. However, when considering the same interval scalars on the same location for both techniques and when high dimensional FE-models ($> 1\text{M DOF}$) are used, the computational cost of modeling the field becomes important. Modelling the field requires commonly a lot of distance measures, that are required to compute the basis functions. For this case study two basis functions have to be computed. For IDW the calculation of two weighting functions on the full model domain Ω are required, such that the total number of distance measures equals:

$$2\left(\frac{L}{h}\right)^2 = 2 \cdot \left(\frac{1}{0.0125}\right)^2 = 12800 \tag{28}$$

With local explicit interval fields in two-dimensions six weighting functions (=three in each dimension) are defined on a local domain $\mathcal{K}$ around there control point. So more weighting function and less distance measures are required due to the smaller domain. In total, the distance measures for this modeling technique are:

$$2\left(2\frac{R_{x1}}{h} + 2\frac{R_{y1}}{h} + 2\frac{R_{x2}}{h} + 2\frac{R_{y2}}{h}\right) = 4\frac{0.1}{0.0125} + 4\frac{0.15}{0.0125} + 4\frac{0.2}{0.0125} + 4\frac{0.1}{0.0125} = 176 \qquad (29)$$

As a result, the computational cost is reduced from 12800 to 176 when using the local explicit interval field formulation.

6 Conclusion

This paper presents an approach to generate a local interval field to represent locally spatial uncertain parameters in FE models up to 2D. To characterise the local character of the interval field this paper proposes two requirements, (1) the weight function is $w > 0$ within a specific region around the control point and $w = 0$ outside that region, (2) the weight function is a monotonically decreasing function towards the edges of that region. The use of quartic splines is proposed, as the selection of weighting functions is limited by these requirements. An academic structural dynamic case study is performed to illustrate the difference between local dependent interval fields and global dependent interval fields using the IDW technique. With this test case, it was shown that the local interval fields model the local dependency much better than fields based on IDW. Another advantage of the local interval fields is that for this case the computational cost (the number of distance measures) is reduced with a factor of 72 in comparison with global interval fields. In this paper, two spatial dimensions and non-overlapping dependency regions in the model domain are considered. The extension to n-dimensions and allowing for overlapping dependency regions requires future research.

Acknowledgments

References

[1] M. Faes and D. Moens, "Recent trends in the modeling and quantification of non-probabilistic uncertainty," *Archives of Computational Methods in Engineering*, pp. 1–39, 2019.

[2] R. L. Muhanna and R. L. Mullen, "Uncertainty in mechanics problems—interval–based approach," *Journal of Engineering Mechanics*, vol. 127, no. 6, pp. 557–566, 2001.

[3] D. Moens, M. De Munck, W. Desmet, and D. Vandepitte, "Numerical dynamic analysis of uncertain mechanical structures based on interval fields," in *IUTAM symposium on the vibration analysis of structures with uncertainties*. Springer, 2011, pp. 71–83.

[4] M. Broggi, M. Faes, E. Patelli, Y. Govers, D. Moens, and M. Beer, "Comparison of bayesian and interval uncertainty quantification: Application to the airmod test structure," in *2017 IEEE Symposium Series on Computational Intelligence (SSCI)*. IEEE, 2017, pp. 1–8.

[5] M. Imholz, D. Vandepitte, and D. Moens, "Derivation of an input interval field decomposition based on expert knowledge using locally defined basis functions," in *1st ECCOMAS Thematic conference on international conference on uncertainty quantification in computational sciences and engineering*, 2015, pp. 1–19.

[6] M. Imholz, D. Vandepitte, and D. Moens, "Analysis of the effect of uncertain clamping stiffness on the dynamical behaviour of structures using interval field methods," in *Applied mechanics and materials*, vol. 807. Trans Tech Publ, 2015, pp. 195–204.

[7] M. Faes and D. Moens, "Identification and quantification of spatial variability in the elastostatic properties of additively manufactured components," in *19th AIAA Non-Deterministic Approaches Conference*, 2017, p. 1771.

[8] A. Sofi and E. Romeo, "A novel interval finite element method based on the improved interval analysis," *Computer Methods in Applied Mechanics and Engineering*, vol. 311, pp. 671–697, 2016.

[9] A. Sofi, G. Muscolino, and I. Elishakoff, "Static response bounds of timoshenko beams with spatially varying interval uncertainties," *Acta Mechanica*, vol. 226, no. 11, pp. 3737–3748, 2015.

[10] D. Wu and W. Gao, "Uncertain static plane stress analysis with interval fields," *International Journal for Numerical Methods in Engineering*, vol. 110, no. 13, pp. 1272–1300, 2017.

[11] B. Xia and L. Wang, "Non-probabilistic interval process analysis of time-varying uncertain structures," *Engineering Structures*, vol. 175, pp. 101–112, 2018.

[12] J. Li, B. Ni, C. Jiang, and T. Fang, "Dynamic response bound analysis for elastic beams under uncertain excitations," *Journal of Sound and Vibration*, vol. 422, pp. 471–489, 2018.

[13] M. Faes and D. Moens, "Identification and quantification of spatial interval uncertainty in numerical models," *Computers & Structures*, vol. 192, pp. 16–33, 2017.

[14] D. Shepard, "A two-dimensional interpolation function for irregularly-spaced data," in *Proceedings of the 1968 23rd ACM national conference*, 1968, pp. 517–524.

[15] D. Moens and M. Hanss, "Non-probabilistic finite element analysis for parametric uncertainty treatment in applied mechanics: Recent advances," *Finite Elements in Analysis and Design*, vol. 47, no. 1, pp. 4–16, 2011.

[16] M. Faes and D. Moens, "On auto-and cross-interdependence in interval field finite element analysis," *International Journal for Numerical Methods in Engineering*, 2019.

[17] M. Faes, R. Callens, and D. Moens, "Adaptive sparse grid approximation for high dimensional interval field construction," in *AIAA Scitech 2020 Forum*, 2020, p. 1418.

[18] R. Callens, M. Faes, and D. Moens, "Local interval fields for spatial inhomogeneous uncertainty modelling," in *ABCM Series on Mechanical Sciences and Engineering*, 2020.

[19] T. Belytschko, Y. Krongauz, D. Organ, M. Fleming, and P. Krysl, "Meshless methods: an overview and recent developments," *Computer methods in applied mechanics and engineering*, vol. 139, no. 1, pp. 3–47, 1996.